LHCb-CONF-2011-012
May 3, 2011

W and Z production at $\sqrt{s} = 7$ TeV with the LHCb experiment

The LHCb Collaboration. [1]

Abstract

We have measured the W and Z boson production cross-sections in proton-proton collisions at a centre-of-mass energy of 7 TeV, using approximately 16.5 pb^{-1} of data. The W and Z bosons are reconstructed from muons with transverse momentum p_T exceeding 20 GeV, pseudorapidity η_μ within $2.0 - 4.5.$, and, in the case of the /zed, a dimuon invariant mass m_Z in the range $81 \leq m_Z \leq 101$ GeV. We obtain:

$$\sigma_Z(2.0 \leq \eta_\mu \leq 4.5, p_T \geq 20, 81 \leq m_Z \leq 101) = 73 \pm 4 \pm 7.3 \text{ pb};$$
$$\sigma_{W+}(2.0 \leq \eta_\mu \leq 4.5, p_T \geq 20) = 1007 \pm 48 \pm 101 \text{ pb};$$
$$\sigma_{W-}(2.0 \leq \eta_\mu \leq 4.5, p_T \geq 20) = 680 \pm 40 \pm 68 \text{ pb},$$

where the first error is statistical and systematic combined, and the second arises from the luminosity uncertainty. The W and Z cross-section ratios $(\sigma_{W+}+\sigma_{W-})/\sigma_Z$ and σ_{W+}/σ_{W-}, and the W charge asymmetry

$$\frac{\sigma_{W+} - \sigma_{W-}}{\sigma_{W+} + \sigma_{W-}},$$

have also been measured within the same kinematic region. Part of this region ($\eta \geq 2.5$) is unique to LHCb, allowing these measurements to test the Standard Model and provide constraints to parton density functions in a new kinematic region. All results are consistent with next-to-leading order theoretical predictions.

[1]Contact author: Tara Shears.

1 Introduction

Measurements of the W and Z [2] cross-sections constitute an important test of the Standard Model in proton-proton collisions with a centre-of-mass energy of 7 TeV. Theoretical predictions have uncertainties of between 3% and 10%, depending on rapidity, where the dominant uncertainty is due to knowledge of the parton distribution functions (PDFs) [1]. Consequently, measurements made by LHCb can test the Standard Model and provide input to constrain the PDFs, both in the unique forward region ($\eta > 2.5$), and in a rapidity region which is in common to ATLAS and CMS ($2 \leq \eta \leq 2.5$).

In this note we report differential cross-section measurements and ratios of W and Z boson production using 16.5 ± 1.7 pb^{-1} of data. We present results for the total W and Z cross-sections inside our kinematic acceptance, where the final state muons have transverse momentum p_T exceeding 20 GeV and lie within pseudorapidities of $2.0 \leq \eta_\mu \leq 4.5$. In addition, muons from Z boson decay are considered within our acceptance if they have an invariant mass m_Z between $81 \leq m_Z \leq 101$ GeV. The cross-sections are also given differentially in five bins of Z boson rapidity, and five bins of W boson muon pseudorapidity. Finally, we present results for the cross-section ratios σ_W/σ_Z and σ_{W+}/σ_{W-}, and the W charge asymmetry

$$\frac{\sigma_{W+} - \sigma_{W-}}{\sigma_{W+} + \sigma_{W-}},$$

within the same lepton pseudorapidity and Z boson rapidity bins. In these cross-section ratios the dependance on luminosity cancels, and in addition some ratios have a reduced dependence on the PDFs allowing the Standard Model to be tested with greater precision. In particular, the W /Z ratio constitutes the single most sensitive test of the Standard Model at the LHC.

This note is organised as follows. The LHCb experiment and trigger are described in the next section. Section 3 describes the selection requirements used to isolate W and Z samples and their performance, and section 4 the relevant reconstruction efficiencies. Section 5 summarises systematic errors sources, and section 6 provides the results and compares to them to theoretical prediction. Section 7 concludes this note.

2 The LHCb experiment

The LHCb experiment, one of four large experiments at the Large Hadron Collider, is a single arm spectrometer instrumented in the pseudorapidity region $1.8 \leq \eta \leq 4.9$. Within this region LHCb is formed of tracking chambers with stations placed on either side of a 4 Tm dipole magnet, two RICH detectors, a calorimetry system consisting of a presampler, scintillating pad detector, electromagnetic and hadronic calorimeters, and five layers of muon chambers. The magnetic field direction can be reversed during operation, although

[2] In this paper, Z refers to both Z and γ^* production around the Z pole.

only data corresponding to one polarity was used in the measurements presented here. Further information about the detector may be found in [2].

Data is triggered using a three level hardware and software based trigger system. Z and W bosons are triggered by requiring that a muon candidate with $p_T > 10$ GeV is present in a collision event. The trigger also places requirements on detector activity, which were introduced to maintain reasonable processing times as the average number of interactions per collision increased. Requirements are made on the maximum allowed hit multiplicity in the main tracking station, the scintillating pad detector and the calorimetry system.

Where possible selection efficiencies and purities are determined directly from data. The Pythia [3] generator and a full detector simulation is used to simulate the processes $Z \rightarrow \mu\mu, Z \rightarrow \tau\tau, W \rightarrow \mu\nu$ and $W \rightarrow \tau\nu$. These samples are used in some purity and efficiency determinations. We compare our measurements to next-to-leading order (NLO) predictions made with the MCFM [4] generator, using the MSTW2008NLO PDF set [5]. We compare Z cross-section measurements in addition to predictions made using the CTEQ6.6 NLO [6] and NNPDF2.0 [7] PDF sets, and the FEWZ [8] generator.

3 Event selection

3.1 $\mathbf{Z} \rightarrow \mu\mu$

Candidate Z events possess two well reconstructed muons which lie within the pseudo-rapidity range $2 \leq \eta \leq 4.5$, with p_T exceeding 20 GeV. Good reconstruction is ensured by placing requirements on the muon track χ^2 probability and relative momentum uncertainty. The invariant mass of the dimuon candidates, $M_{\mu\mu}$ must lie within $81 \leq M_{\mu\mu} \leq 101$ GeV. As these selection criteria define the kinematic region of our measurement, we take the selection efficiency and acceptance as 1.0. The invariant mass distribution of candidate events is shown in figure 1. We select 833 candidates. The distribution is fitted to a Crystal Ball function to represent signal, on an exponential to represent background. The fitted mass (90.7 ± 0.1 GeV) and width (3.2 ± 0.1 GeV) are in accordance with expectation.

3.1.1 Backgrounds

We consider the following background sources:
(i) $Z \rightarrow \tau\tau$ where both taus decay leptonically to muons;
(ii) b and c events ("heavy flavour"), with two semileptonic decays;
(iii) generic QCD events where pions or kaons either decay in flight or punch through the detector to be falsely identified as muons.

We estimate a contribution of 0.2 ± 0.2 Z decays to tau, from simulation. Real data is used to estimate the heavy flavour and generic QCD backgrounds.

The heavy flavour component is estimated by considering events containing two muon candidates with an impact parameter significance ip_{sig} greater than five. We require that

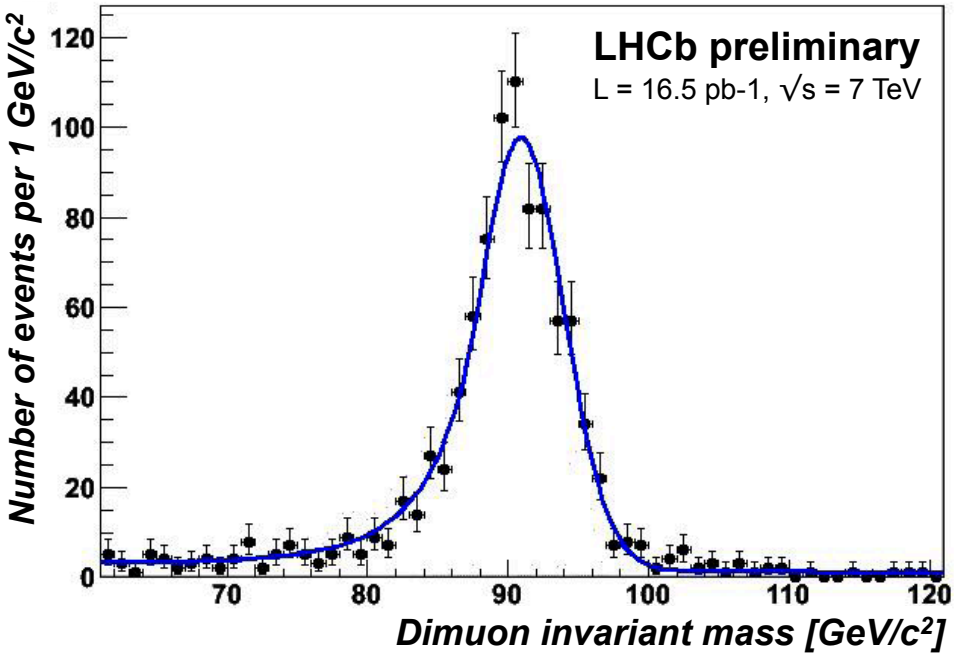

Figure 1: Invariant mass of selected Z candidates. The data points are fitted to a Crystal Ball function to represent signal, on an exponential to represent background.

these muons are not isolated by asking that the vector summed p_T of all tracks inside a cone of radius $r = \sqrt{\Delta\eta^2 + \Delta\phi^2} = 0.5$ surrounding the muon, r_{cone}, should be more than 5 GeV. We do not expect signal to contribute to this region. The invariant mass distribution of these events is peaked at low values and falls rapidly. From this distribution we estimate a heavy flavour contamination of 1 ± 1 event.

The generic QCD event background is determined by considering the rate at which pions and kaons are falsely identified as muon candidates, as a function of momentum. This muon misidentification rate is used to weigh the number of events in a minimum bias triggered data sample, where all requirements are imposed aside from muon identification, to derive an estimated number of candidates from this source. We find that the number of candidates we expect is negligible. The total background estimate is taken as 1.2 ± 1.2 events.

3.2 $\mathbf{W} \rightarrow \mu\nu$

Candidate W events possess one well reconstructed isolated muon candidate with a p_T greater than 20 GeV within $2 \leq \eta \leq 4.5$. As backgrounds to the W analysis are larger than for the Z analysis we impose additional criteria on muon isolation, and ask that it is consistent with the primary vertex. We also apply slightly harsher requirements on track reconstruction quality. Isolation is imposed by requiring that r_{cone} should be less than 2 GeV. The impact parameter significance, ip_{sig} of the muon must be less than 2 to reduce backgrounds from heavy flavour production.

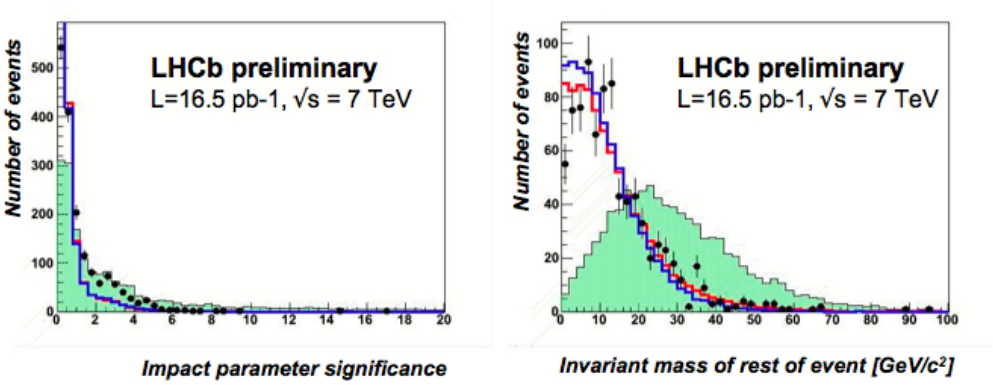

Figure 2: Distributions for (left) impact parameter significance and (right) the invariant mass of all tracks in the event aside from the muon: Z data (points); Z simulation (red histogram); W simulation (blue histogram); QCD background (green histogram).

As the neutrino is unreconstructed inside LHCb, two requirements are placed on the rest of the event to select candidates consistent with W production. The invariant mass of tracks other than the muon in the event must be less than 20 GeV. The vector summed p_T of all tracks apart from the muon must be less than 10 GeV. After these requirements are made we have 7624 (5732) W^+ (W^-) candidates.

The efficiency of the selection is determined from data. We use Z event data, where both muons have $p_T > 20$ GeV, and remove one of the muons to simulate a neutrino. We find that Z and W simulated events give consistent variable shapes, with the exception of the event invariant mass which shows a small difference. Figure 2 shows distributions for ip_{sig} and the event invariant mass. It can be seen that the Z event data, Z and W simulated data distributions are similar. Also shown is the estimated QCD and heavy flavour background shape, which is obtained as explained in the next section.

We determine a selection efficiency of $\epsilon^W_{sel} = 0.55 \pm .01$. The acceptance of this selection is also 1.0.

3.2.1 Backgrounds

We consider the following background sources:
(i) $Z \to \mu\mu$ where one of the muons goes outside of the LHCb acceptance;
(ii) $Z \to \tau\tau$ where one tau decays leptonically with a muon in the final state inside the LHCb acceptance;

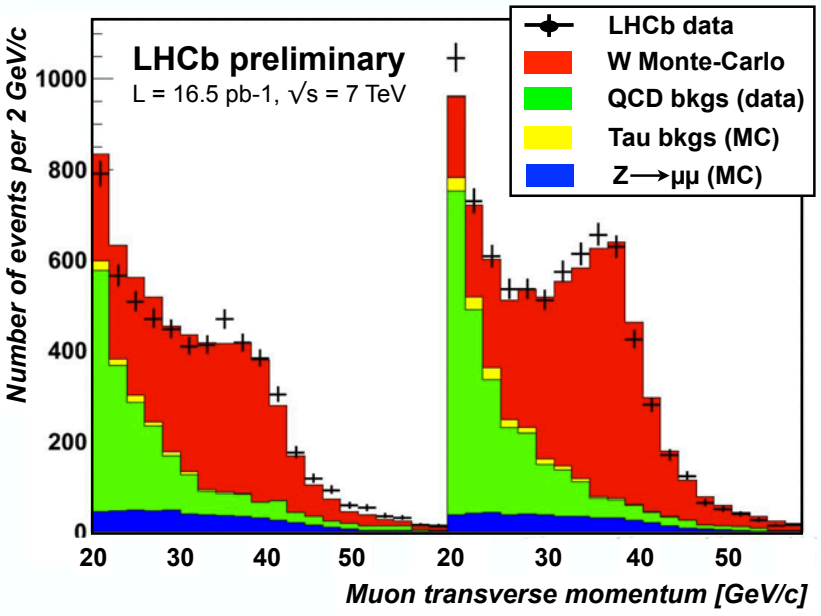

Figure 3: Distribution of muon p_T for negative (left) and positive (right) charged leptons. The estimated W contribution is in red, the Z background is in blue, the tau background in yellow, and the QCD background in green.

(iii) $W \to \tau\nu$ where the tau decays leptonically to a muon and neutrinos;
(iv) b and c events containing semileptonic decays with a muon in the final state;
(v) generic QCD events where pions or kaons either decay in flight or punch through to give muons.

The signal yield is estimated by fitting the lepton p_T spectrum to the shapes expected for signal (from simulation) and each background class. The shapes for backgrounds (i) to (iii) are estimated using simulation, which is normalised and fixed to the rate observed for $Z \to \mu\mu$ in data. The shapes for backgrounds (iv) and (v) are found directly from data by anti-cutting on selection variables to enrich these sources, and their normalisation allowed to float in the fit.

The W selected data and the result of the fit is shown in Figure 3. The fit estimates that $34 \pm 1\%$ of the sample comes from W^+, $26 \pm 1\%$ comes from W^- and $31 \pm 1\%$ is due to the QCD background. The number of background events is given in table 1.

	$W+$	$W-$
N_W^{tot}	7624	5732
$W \to \tau\nu$	151	90
$Z \to \tau\tau$	2	2
$Z \to \mu\mu$	460	506
Heavy flavour and misidentified π/K	2194 ± 150	1654 ± 150
N_W	4817 ± 165	3480 ± 161

Table 1: Number of W candidate, background, and estimated signal events in the W cross-section analysis.

4 Cross-section determination

The cross-section, σ_Z, for Z boson production in a rapidity region, Δy can be written

$$\sigma_{Z\to\mu\mu}(\Delta y) = \frac{N_{tot}^Z - N_{bkg}^Z}{\epsilon_Z L},$$

where N_{tot}^Z is the number of selected events, N_{bkg}^Z is the estimated number of background events, L is the integrated luminosity corresponding to the selected events, and ϵ_Z is the overall efficiency for selecting signal events. This efficiency can be expressed as a product of: an acceptance factor, A^Z, which is the proportion of events that would produce two reconstructible objects inside the given rapidity range; a trigger efficiency, ϵ_{trig}^Z, which is the probability of triggering on such an offline selected event; a tracking efficiency, ϵ_{track}^Z, which is the probability of reconstructing both Z decay products as tracks; a muon reconstruction efficiency, ϵ_{muon}^Z, which is the probability of identifying both tracks as muons; and a selection efficiency, ϵ_{sel}^Z, which is the probability of these muons passing additional selection cuts.

Similarly, we express the cross-section for W production, σ_W, in a lepton pseudorapidity interval $\Delta\eta$ as

$$\sigma_{W\to\mu\nu}(\Delta\eta) = \frac{N_{tot}^W - N_{bkg}^W}{\epsilon_W L},$$

where now $\epsilon_W = A^W \epsilon_{trig}^W \epsilon_{track}^W \epsilon_{muon}^W \epsilon_{sel}^W$, using the same notation as above, but with a W superscript or subscript in place of a Z and where the efficiencies correspond to one, and not two muons.

These efficiencies are determined from data and are described in the following subsections. We measure W and Z production cross-sections with the kinematic requirement that both muons have transverse momenta p_T above 20 GeV and pseudorapidities η between 2 and 4.5. To minimise the dependance on theory when extrapolating over unmeasured regions we do not correct this to a 4π measurement. We choose the region $2 \leq \eta \leq 4.5$ to minimise detector edge effects which may not be well simulated. It should be noted that the measurements we quote are uncorrected for final state radiation.

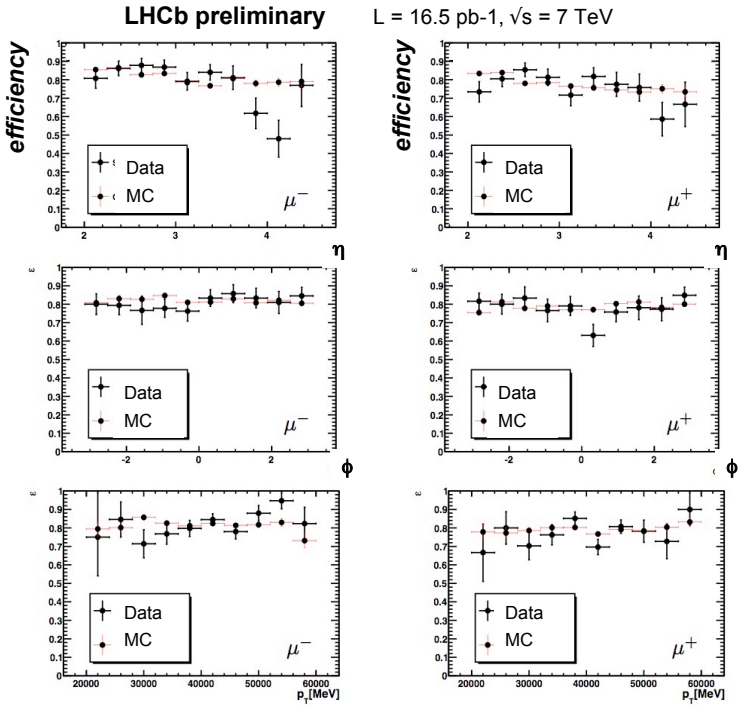

Figure 4: Trigger efficiency for data (black points) and Monte Carlo (red points) for (left) μ^+ and (right) μ^-, shown as a function of η (top), ϕ (centre) and p_T (bottom).

4.1 Trigger Efficiency

The trigger efficiency is determined from data using Z candidates obtained using the selection described above. One muon is required to fire the single muon trigger. The other muon is examined to see how often this also fires the single muon trigger. We determine the trigger efficiency as a function of muon charge, p_T, η and ϕ. No evidence for any dependence on these variables is found, as can be seen in figure 4. We find $\epsilon^W_{trig} = 0.73 \pm 0.01$ and $\epsilon^Z_{trig} = 0.86 \pm 0.01$.

4.2 Track finding efficiency

The track finding efficiency is determined from data using Z candidates, using a tag and probe method. The tag muon is defined as that which fired the single muon trigger, and which passes the standard selection criteria. The probe muon is defined as a stub (a track segment reconstructed in the muon system based on finding hits in all five stations). Where possible, hits in a tracking chamber (TT) not used in the standard track finding definition are attached to the stub to improve resolution. Those tag-probe muon combinations with an invariant mass consistent with the Z boson are used to determine the efficiency, by considering the number of times that the muon stub has a standard track

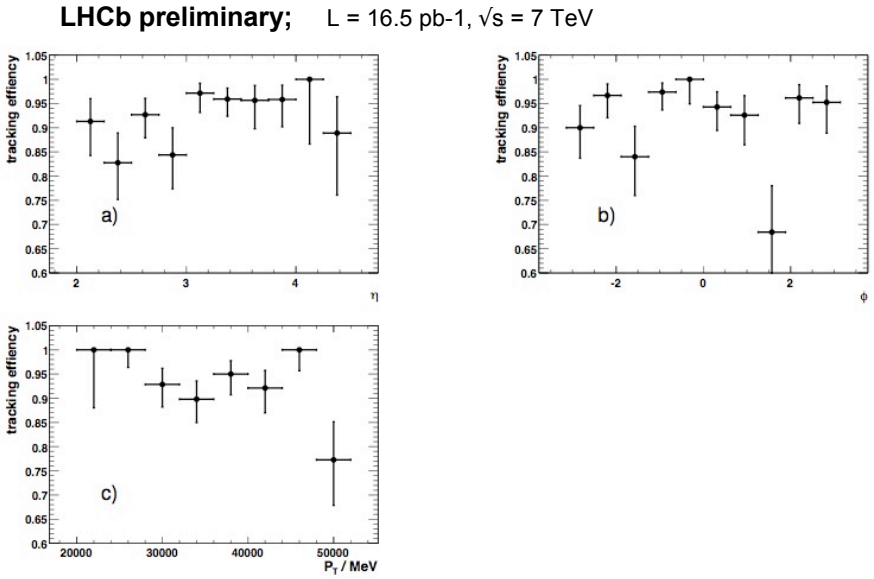

Figure 5: Track finding efficiency for data (black points), shown as a function of (a) η, (b) ϕ and (c) p_T.

associated to it. There is no evidence for charge bias or any efficiency dependance with p_T or ϕ. The efficiency shows some dependence on η, as shown in figure 5. For the analysis presented here we determine the efficiency separately for the regions $\eta < 3$ and $\eta > 3$, and apply the appropriate value accordingly. We find

$$\epsilon^{W+}_{track} = 0.73 \pm 0.03, \epsilon^{W-}_{track} = 0.78 \pm 0.03,$$

and

$$\epsilon^{Z}_{track} = 0.83 \pm 0.03.$$

The difference between W^+ and W^- efficiency is due to the different decay lepton pseudorapidity distributions. The difference between W and Z track finding efficiency is due to the more restrictive track quality criteria which have been applied to muons from W decay.

4.3 Muon identification efficiency

The muon identification efficiency is determined from data using Z candidates, using a tag and probe method. Here the tag muon is defined as before. The probe is now an identified

track with $p_T > 20$ GeV. Tag-probe combinations with an invariant mass consistent with a Z boson are used to determine the efficiency, by considering the number of times the probe track is identified as a muon. There is no evidence for charge bias or that the efficiency depends on p_T, η or ϕ. We find that the efficiency for reconstructing one muon (ϵ^W_{muon}) is 0.982 ± 0.005 and two muons (here defined as ϵ^Z_{muon}) is 0.965 ± 0.007.

4.4 Luminosity

The luminosity is measured by two methods, a Van Der Meer scan [9] where colliding beams are moved transversely across each other to determine the beam profile, and a beam gas method [10], where reconstructed beam-gas interaction vertices near the beam crossing point determine the beam profile. Both methods give similar results and are estimated to have a precision of order 10%. We estimate that the dataset analysed here corresponds to an integrated luminosity of 16.5 ± 1.7 pb^{-1}.

5 Systematic errors

Sources of systematic error that have been considered for this analysis are: luminosity; background estimates; efficiency determination. The uncertainty on the luminosity has been discussed before. The uncertainty on the background estimates and efficiency determinations will be described in the following subsections.

5.1 Background estimates

Background estimates are taken mostly from data. Where simulated events have been used, these have been normalised by the observed rate of selected Z events. For the Z analysis backgrounds are low and we take the statistical error of our estimates as the systematic error. For the W analysis we determine backgrounds by fitting p_T distributions to the distribution observed in data. If our assumed background shapes are wrong, this yields a systematic error. We estimate our background shapes from simulation for $Z \to \mu\mu$, $Z \to \tau\tau$ and $W \to \tau\nu$, and by anticutting on selection variables to obtain shapes for the heavy flavour and QCD components combined. We repeat the muon p_T fit using template shapes for the latter obtained by anticutting on each selection variable in turn. The largest variation observed ($3 - 5\%$) is taken to be the systematic error due to this method.

5.2 Efficiency determinations

Efficiencies are determined directly from data. We take the statistical error of each efficiency determination as a conservative estimate of the systematic error, as we have already checked for charge bias and dependance on ϕ, η and p_T, and taken any observed dependance into account.

Source	σ_Z	σ_{W+}	σ_{W-}
Background	0.1	3	5
Trigger efficiency	1	1	1
Muon id efficiency	0.7	0.5	0.5
Track efficiency	4	4	4
Selection efficiency	n/a	2	2
Luminosity	10	10	10
Stat. error	4	1	1

Table 2: Summary of the systematic error contributions (% uncertainty) to the cross-section measurement (all given to 1 significant figure), together with the statistical error.

The systematic errors are summarised in table 2. It can be seen that the luminosity uncertainty dominates.

6 Results

In this section we summarise our results and compare them to theoretical predictions.

6.1 Inclusive and differential cross sections

We find:

$$\sigma_Z(2.0 < \eta_\mu < 4.5, p_T > 20, 81 < m_Z < 101) = 73 \pm 4 \pm 7.3 \text{ pb},$$

$$\sigma_{W+}(2.0 < \eta_\mu < 4.5, p_T > 20) = 1007 \pm 48 \pm 101 \text{ pb},$$

$$\sigma_{W-}(2.0 < \eta_\mu < 4.5, p_T > 20) = 680 \pm 40 \pm 68 \text{ pb},$$

where the first error is statistical and systematic combined (aside from the luminosity uncertainty), and the second comes from the luminosity determination.

The Z (W) cross-sections have also been determined in five boson rapidity (lepton pseudorapidity) bins, of size 0.5 between 2 and 4.5. The differential cross-section for Z production is shown in figure 6. The differential W cross-sections are used to work out the W charge asymmetry.

6.2 Cross-section ratios

We have calculated the following ratios of cross-sections:

$$\sigma_{W+}/\sigma_{W-} = 1.48 \pm 0.11;$$

$$\frac{\sigma_{W+}(2.0 < \eta_\mu < 4.5) + \sigma_{W-}(2.0 < \eta_\mu < 4.5)}{\sigma_Z(2.0 < y < 4.5)} = 23.1 \pm 1.5;$$

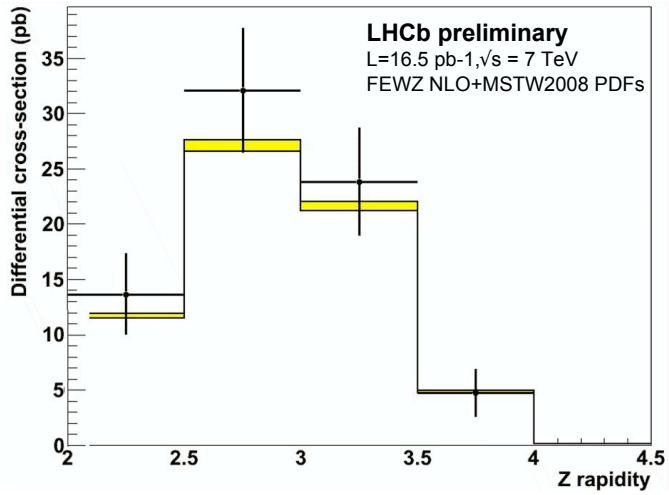

Figure 6: Differential cross-section for Z boson production. The points are the measured data, the error bars the statistical and systematic error combined in quadrature, and are superimposed on NLO predictions given by the FEWZ generator. The shaded area denotes the uncertainty due to the MSTW08 PDFs.

where the error is statistical and systematic combined. We assume that the background uncertainty is correlated in the ratio of the W^+ to W^- boson production, but that the uncertainty on the efficiency is anticorrelated, allowing for differences in the positive and negative tracking and triggering efficiencies. The uncertainty on the luminosity cancels in the ratio. The uncertainty on the ratio of W to Z boson production has been found by adding all uncertainties except for luminosity in quadrature.

We have also calculated the W charge asymmetry:

$$A_W = \frac{\sigma_{W+} - \sigma_{W-}}{\sigma_{W+} + \sigma_{W-}},$$

in five bins of lepton pseudorapidity. Results are given in table 3 and shown in figure 7. Unlike in the central region, where for ATLAS and CMS this distribution is almost flat, in the forward region the asymmetry changes sign, showing the differing helicities of the couplings of the leptons. The experimental uncertainties have been found assuming the background uncertainty is correlated, but the uncertainty on the positive and negative efficiencies is anticorrelated. The main theory uncertainty comes from the difference in the u and d valence quark parton density functions.

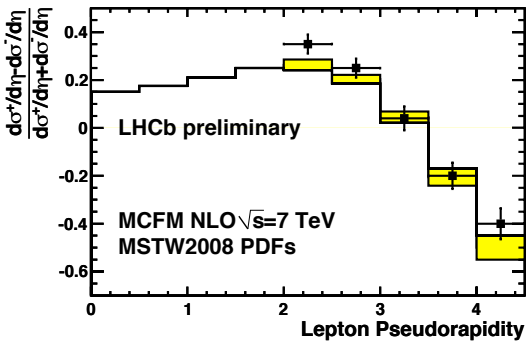

Figure 7: W charge asymmetry in bins of lepton pseudo-rapidity compared to the MCFM prediction. The shaded area is the uncertainty arising from the MSTW08NLO PDF set.

η_μ	A_W
2.0 - 2.5	0.35 ± 0.04
2.5 - 3.0	0.25 ± 0.04
3.0 - 3.5	0.04 ± 0.05
3.5 - 4.0	-0.20 ± 0.055
4.0 - 4.5	-0.40 ± 0.065

Table 3: W charge asymmetry values for the lepton pseudorapidity bins considered.

6.3 Comparison to theory

We compare our results to NLO prediction, using the MCFM generator [4] with the MSTW2008NLO PDF set [5].

The uncertainty on each prediction is a combination of the NLO calculation and the 90% eigenvalue envelope of the PDF sets. Table 4 summarises our experimental results and the predictions for W and Z . Also tabulated for σ_Z are NLO predictions obtained using the FEWZ [8], and MCFM generators using the CTEQ6.6 NLO [6] and NNPDF2.0 [7] PDF sets in addition. The results agree well with NLO prediction in all cases.

The comparison is shown graphically in Figure 8. The precision of the inclusive cross-section measurements will improve when a more precise determination of luminosity is available. The cross-section ratios, which are independent of experimental luminosity, will constitute a very sensitive test of the Standard Model with increased statistics.

7 Conclusions

The cross-sections and ratios of W and Z bosons have been measured using 16.5 pb^{-1} of data. The luminosity uncertainty of 10% dominates the precision of the cross-section measurements. This luminosity uncertainty cancels in the cross-section ratios, which

Generator	PDF Set	σ(Z)	$\sigma(W+)$	$\sigma(W-)$	σ(W)/σ(Z)	$\sigma(W+)/\sigma(W-)$
FEWZ	MSTW08NLO	$65.7^{+2.9}_{-2.5}$				
	CTEQ66NLO	$66.6^{+2.6}_{-2.4}$				
	NNPDF2.0	65.0 ± 2.4				
MCFM	MSTW08NLO	$65.5^{+2.8}_{-2.5}$	851 ± 35	656 ± 30	23.1 ± 0.2	1.30 ± 0.04
Data		$73 \pm 4 \pm 7.5$	$1007 \pm 48 \pm 101$	$682 \pm 40 \pm 68$	23.1 ± 1.5	1.48 ± 0.11

Table 4: Summary of theoretical calculations for various NLO generators and PDF sets where the uncertainty quoted combines the precision of the calculation and the 90% PDF uncertainty. The quoted cross-sections require that the leptons have $p_T > 20$GeV and pseudorapidities between 2 and 4.5.

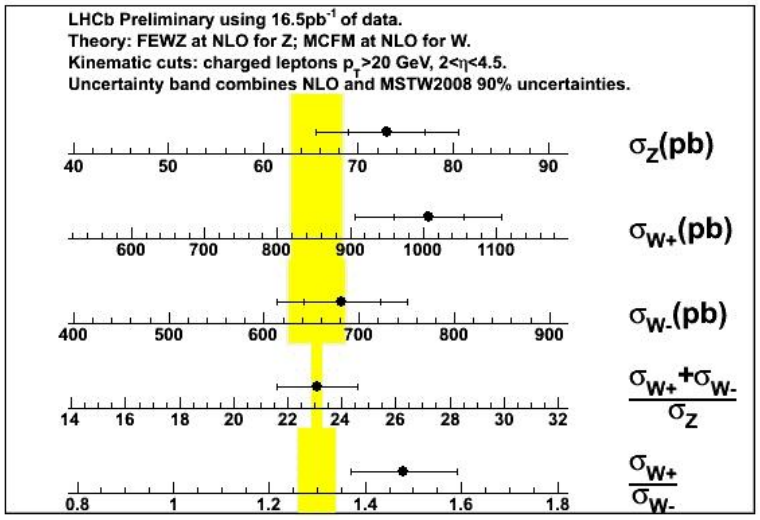

Figure 8: Z , W + and W - cross-section measurements and ratios compared to the MCFM NLO prediction. The inner uncertainty combines the statistical and systematic experimental uncertainties. The outer uncertainty bar includes the luminosity uncertainty. The yellow bar is the theoretical uncertainty.

provide a more precise test of Standard Model predictions and probe of parton density functions. All results are consistent with NLO predictions.

References

[1] See, for example, R. Thorne *et al.*, arXiv:0808.1847 [hep-ph], published online under [doi:10.3360/dis.2008.30].

[2] A. Augusto Alves *et al.* JINST 3:S08005, 2008.

[3] T. Sjstrand *et al.*, Computer Phys. Commun. **135** 238, 2001.

[4] J. M. Campbell, R. K. Ellis, Phys. Rev. **D62**:114012, 2000.

[5] A. D. Martin *et al.* Eur. Phys. J. **C63**:189-285, 2009.

[6] P. M. Nadolsky *et al.* Phys. Rev. **D78**:013004, 2008.

[7] R. D. Ball *et al.* Nucl. Phys. **B838**:136-206, 2010.

[8] R. Gavin *et al.* arXiv:1011.3540 [hep-ph]

[9] S. Van Der Meer, ISR-PO/68-31, 1968.

[10] M. Ferro-Luzzi, CERN-PH-EP/2005-023 (2005).